

REPORT DOCUMENTATION PAGE				Form Approved OMB No. 0704-0188	
The public reporting burden for this collection of information is estimated to average 1 hour per response, including the time for reviewing instructions, searching existing data sources, gathering and maintaining the data needed, and completing and reviewing the collection of information. Send comments regarding this burden estimate or any other aspect of this collection of information, including suggestions for reducing the burden, to the Department of Defense, Executive Service Directorate (0704-0188). Respondents should be aware that notwithstanding any other provision of law, no person shall be subject to any penalty for failing to comply with a collection of information if it does not display a currently valid OMB control number.					
PLEASE DO NOT RETURN YOUR FORM TO THE ABOVE ORGANIZATION.					
1. REPORT DATE (DD-MM-YYYY) 7/1/2012		2. REPORT TYPE Final Technical Report		3. DATES COVERED (From - To) 09/01/2010 -2/29/2012	
4. TITLE AND SUBTITLE Development of an Acetate- or Sugar-fed Microbial Power Generator for Military Bases				5a. CONTRACT NUMBER N00014-10-M-0231	
				5b. GRANT NUMBER N00014-10-M-0231	
				5c. PROGRAM ELEMENT NUMBER	
6. AUTHOR(S) Dr. Bruce E. Rittmann Dr. César I. Torres Dr. Rosa Krajmalnik-Brown Dr. Sudeep Popat Dr. Prathap Parameswaran				5d. PROJECT NUMBER	
				5e. TASK NUMBER	
				5f. WORK UNIT NUMBER	
7. PERFORMING ORGANIZATION NAME(S) AND ADDRESS(ES) Arizona State University Office for Research and Sponsored Projects B163 PO Box 873503 Tempe AZ 85287-3503				8. PERFORMING ORGANIZATION REPORT NUMBER  KXS-0049-2	
9. SPONSORING/MONITORING AGENCY NAME(S) AND ADDRESS(ES) Office of Naval Research Attn: Linda Chrisey ONR 341 875 North Randolph St Arlington, VA 22203-1995				10. SPONSOR/MONITOR'S ACRONYM(S)  ONR	
				11. SPONSOR/MONITOR'S REPORT NUMBER(S)	
12. DISTRIBUTION/AVAILABILITY STATEMENT No distribution limitations					
13. SUPPLEMENTARY NOTES N/A					
14. ABSTRACT Military missions often require the transport of fuel, such as diesel, to military bases in remote locations. The delivery of such flammable fuels is very expensive and dangerous, particularly in hostile environments. An ideal fuel source for military missions would be non-flammable, renewable, and readily available. Microbial fuel cells (MFCs) are a new technology in which microbes convert organic compounds (sugars, alcohols, complex wastes) directly into electrical power. Microbial catalysis at the anode opens up the possibility to use non-flammable organic material as a fuel-cell fuel, not just H <sub>2</sub> , as with a conventional fuel cell. MFCs have been proven to produce significant power densities (>1 W/m <sup>2</sup> of electrode) at a small scale. In our work, we designed a prototype MFC as a module for future large-scale applications that is capable of producing high power densities with minimal potential losses. In order to achieve this goal, we tested various materials, MFC designs, microbial community optimization, and transport limitations. Our results show the need to better optimize ion transport in MFCs, while making significant progress towards achieving an efficient conversion of sucrose to electricity.					
15. SUBJECT TERMS MFCs - Microbial Fuel Cells ARB - Anode respiring bacteria					
16. SECURITY CLASSIFICATION OF:			17. LIMITATION OF ABSTRACT		18. NUMBER OF PAGES
a. REPORT	b. ABSTRACT	c. THIS PAGE	UU		19a. NAME OF RESPONSIBLE PERSON Bruce E. Rittmann
U	U	U			19b. TELEPHONE NUMBER (Include area code)
					32

**Technical Report for the Office of Naval Research**

**Title:** Development of an Acetate- or Sugar-fed Microbial Power Generator  
for Military Bases

**PIs:** Dr. Bruce Rittmann, Dr. César Torres, and Dr. Rosa Krajmalnik-Brown

**Other Contributors:** Dr. Sudeep Popat, and Dr. Prathap Parameswaran

**Affiliation:** Swette Center for Environmental Biotechnology, Biodesign Institute,  
Arizona State University

**Award #:** N00014-10-M-0231

20120703300

The world is in urgent need of renewable energy sources. Fossil fuel reserves are depleting worldwide, and the harmful effects of their use on global climate are increasingly becoming evident. Fossil fuels dominate the United States' energy portfolio, and thus finding local, renewable sources is a top priority to ensure energy security of our country (U. S. DOE, 2009). Challenges related to energy are also evident in the U.S. military, which consumes 395,000 barrels of oil every day (Warner and Singer, 2009). Transport of fossil fuels to remote places in hostile environments represents a significant cost and security risk to the military.

An ideal fuel for military missions is one that would be readily available, and renewable. In addition, a non-flammable fuel would reduce the risks associated with its transportation. Our project explores one possible solution to this requirement. We investigated the possibility of using microbial fuel cells (MFCs) to generate electrical power at military bases from inexpensive, non-combustible fuels. MFCs are a class of fuel cells in which conversion of energy present in chemical bonds is recovered in usable form without any combustion. In MFCs specifically, bacteria grow on an anode and convert organic fuels to generate an electrical current. The electrons move through a circuit to the cathode where oxygen ( $O_2$ ) is reduced to water on metal catalysts. Unlike other widely developed fuel cells (e.g., PEM fuel cells) that use hydrogen ( $H_2$ ), a combustible gas as the fuel, MFCs have the versatility of being able to convert biodegradable organic material.

The concept of MFCs is relatively new and holds great promise for energy recovery from organic materials, especially various kinds of wastes. Figure 0.1 is a schematic of how an MFC works. Inside an MFC, anode-respiring bacteria (ARB) catalyze the conversion of organic matter directly into electricity. ARB form a biofilm on the surface of an electrode (the anode) and transfer electrons to the anode from the oxidation of a variety of electron donors, such as glucose, ethanol, acetic acid, and others (Liu et al., 2005; Logan et al., 2006; Torres et al., 2007). A key concept in an MFC is that ARB transfer electrons to the electrode instead of directly transferring them to a terminal electron acceptor. Therefore, the electrons must pass through a circuit where energy is drawn before they finally reach the cathode, the location where they reduce  $O_2$  to form water. To separate the anode and cathode compartments, a membrane capable of transferring protons ( $H^+$ ) or hydroxides ( $OH^-$ ) is usually used; most MFC studies use a proton exchange membrane (PEM) for this purpose (Chaudhuri and Lovley, 2003; Logan et al., 2006), but we use an anion-exchange membrane to obtain important benefits.

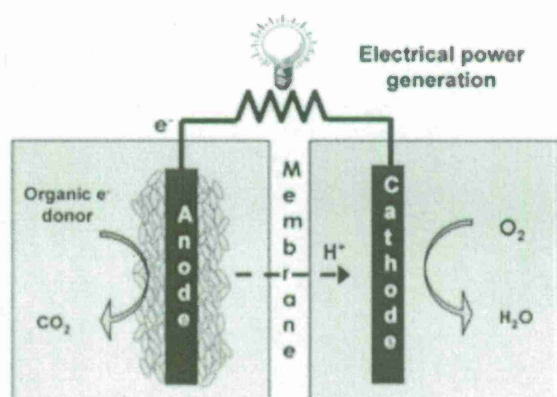


**Figure 0.1.** Schematic of the components in an MFC. The anode compartment (left) holds an anode in which anode-respiring bacteria (ARB) grow as a biofilm. In the cathode compartment (right), air is fed to supply O<sub>2</sub> as oxidant. An electron flow from anode to cathode generates electrical power. Ions (expressed as H<sup>+</sup> in the figure) are transported between the compartments to provide electroneutrality through an ion-exchange membrane.

An MFC is a hybrid between an electrochemical cell and a biofilm reactor. In order to optimize its performance and maximize its efficiency, a novel MFC design that allows bacteria to grow, while minimizing potential losses in the electrical and ionic circuit of the fuel cell, is needed. First, the ARB require a high surface area, as they grow as a biofilm, and have required growth conditions (e.g., water, neutral pH, nutrients) that must be available in the anode compartment. A high ratio of biofilm surface area to MFC volume allows a high output-power density. Second, fuel cells should be developed in a compact design, where the distance between anode and cathode is <1 cm, in order to minimize energy losses. Thus, a main goal for this project was to design an MFC capable of producing high power densities with minimal potential losses.

For military operations, a simple fuel source that is easily consumed by ARB is desirable. In our project, we studied two non-flammable, renewable fuels that are cheap and widely available: acetate and sucrose. We selected these two fuels because of their wide availability in the world market, their relative low cost, and the capability to produce high power densities from them in laboratory MFCs. While both these fuels have low energy density compared to gaseous fuels such as H<sub>2</sub> or CH<sub>4</sub>, as well as liquid fuels such as gasoline and diesel (Perlack et al., 2005), they are non-combustible and thus represent a possible cost savings in transportation due to lower safety standards required.

As shown in Figure 0.1, the MFC has various components that must be optimized for its operation. These include: (1) the ARB, which catalyze the fuel oxidation, (2) the anode and



cathode materials, and (3) the ion-exchange membrane. In this project, we targeted optimization of each component of MFCs and then used these components in novel reactor designs that yield high power densities.

### **Major Achievements of this Project**

Described below briefly is the organization of the report and a description of the major achievements made in the design of MFCs.

*1) Characterization and selection of anode materials:* In this section, we describe our efforts to optimize the anode material for growth of ARB. We tested graphite and stainless steel as possible materials to grow ARB and evaluated current production on both.

*2) Characterization and selection of anion exchange membrane:* In this section, we describe the various characterizations that we performed on commercially available anion exchange membranes in terms of their resistance to ion transport. We also discuss why it is important to use an anion exchange membrane, as opposed to the more commonly used proton exchange membrane.

*3) Construction and performance of first MFC prototype:* In this section, we describe the performance of the first flat-plate MFC prototype that we constructed, for which we used acetate as the fuel. We show, using images, how we step-by-step constructed the MFC and how we envision the various components to be used in an efficient design. We also show how the cathode limits the power densities in MFCs, which led to the studies described later.

*4) Characterization of anode and Ohmic losses in MECs:* In this section, we describe how we used a microbial electrolysis cell (MEC), in which additional voltage is added to overcome any cathodic limitations, to study other components of our design in further detail. This allowed us to study the energy losses at the anode and due to ion transport. We determined that these losses are small, and high current densities can be achieved with minimal energy losses as long as (i) a high surface area electrode is available for ARB to grow on, and (ii) the distance between the anode and the cathode is minimized to  $<0.5$  cm.

*5) Identification and characterization of cathodic overpotentials:* This section describes the in-depth studies we conducted to determine the reasons leading to cathodic limitations in MFCs. We used platinum catalyst in all our cathodes. We know that platinum catalysts allow current densities that are 2 to 3 orders of magnitude higher in chemical fuel cells. We describe the

importance of the transport of  $\text{OH}^-$  (a product of the  $\text{O}_2$  reduction reaction) in cathode performance, and we show that cathode performance can be improved either by changing some of the materials of construction or selecting a buffer that can be transported rapidly and act as an  $\text{OH}^-$  carrier out of the cathode surface.

*6) Development of co-culture for enhanced energy recovery from sucrose:* Efficient ARB such as *Geobacter* sp. use acetate primarily as their electron donor. Thus, to convert a more complex fuel, such as sucrose, additional fermentative bacteria are needed. In this section, we describe our efforts in developing a homo-acetogenic culture that converts sucrose mostly to acetate, which can be further converted to electrical current by *Geobacter* sp. We also show how a co-culture leads to enhanced recovery of electrons (>80%) in an MEC.

This project led to publication of two peer-reviewed journal papers listed below:

1. S. C. Popat, D. Ki, B. E. Rittmann, C. I. Torres (2012). Importance of  $\text{OH}^-$  transport from cathodes in microbial fuel cells. *ChemSusChem*, 5, 1071-1079.
2. D. R. Bond, S. M. Strycharz-Glaven, L. M. Tender, C. I. Torres (2012). On electron transport through *Geobacter* biofilms. *ChemSusChem*, 5, 1099-1105.

### **1. Characterization and selection of anode materials:**

Several materials have been used successfully as anodes to grow ARB. Carbon-based electrodes are the most popular, and we have extensively used graphite and carbon fibers as anode support for ARB growth in our laboratory (Torres et al., 2008a; Torres et al., 2008c; Lee et al., 2010). Other research groups have used these and other carbon-based materials, such as activated carbon (He et al., 2006). Non-corrosive metals, such as stainless steel and gold, have also been used as an MFC anode (Richter et al., 2008; Dumas et al., 2008).

A main requirement for a good anode material is to provide a high surface area for ARB biofilms to grow. Maximizing ARB growth area maximizes volumetric current densities in MFCs. Carbon fibers are lightweight, inexpensive, and have a 7-12  $\mu\text{m}$  diameter, which allows a high surface-to-volume ratio. However, they are not as conductive as metal alloys such as stainless steel, and, thus, a current collector is required to build the anode. Instead, stainless steel fibers could possibly serve as an anode material, also allowing more efficient current collection. Although stainless steel fibers are more expensive and heavier than carbon fibers, we hypothesized that they would allow high current densities at lower potential losses due to their high conductivity, if ARB are able to grow well on them. Therefore, we evaluated carbon and stainless steel anodes in the first phase of this project to select the best material for MFC modules.

We compared the performances of acetate-fed microbial electrolysis cells (MECs) with graphite rods and stainless steel meshes, selected as simple anodes to rapidly test the affinity of ARB towards them. We selected meshes made from 316-grade stainless steel for these studies. We conducted several trials with the MECs, similar to as we have done in the past (Torres et al., 2008b; Parameswaran et al., 2009), and the performance of one set of MECs is reported in Figure 1.1. As expected with graphite rod anodes, we were able to achieve current densities of  $\sim 11 \text{ A m}_{\text{an}}^{-2}$  at a poised anode potential of  $-0.4 \text{ V vs. Ag/AgCl}$  (Figure 1.1(a)) when inoculated with anaerobic digested sludge as inoculum. This is consistent with our previous results using graphite as anode material, wherein we have been able to enrich for *Geobacter* spp. and obtain similar current densities at this poised potential (Torres et al., 2009). We were unable to enrich for efficient ARB from the same anaerobic digested sludge inoculum using a stainless steel mesh anode at a poised potential of  $-0.4 \text{ V vs. Ag/AgCl}$  (data not shown). When we used enriched ARB cultures as inoculum in stainless steel anode MECs, we observed current generation, but current densities were an order of magnitude lower than for graphite rod MECs (Figure 1.1 (b)).

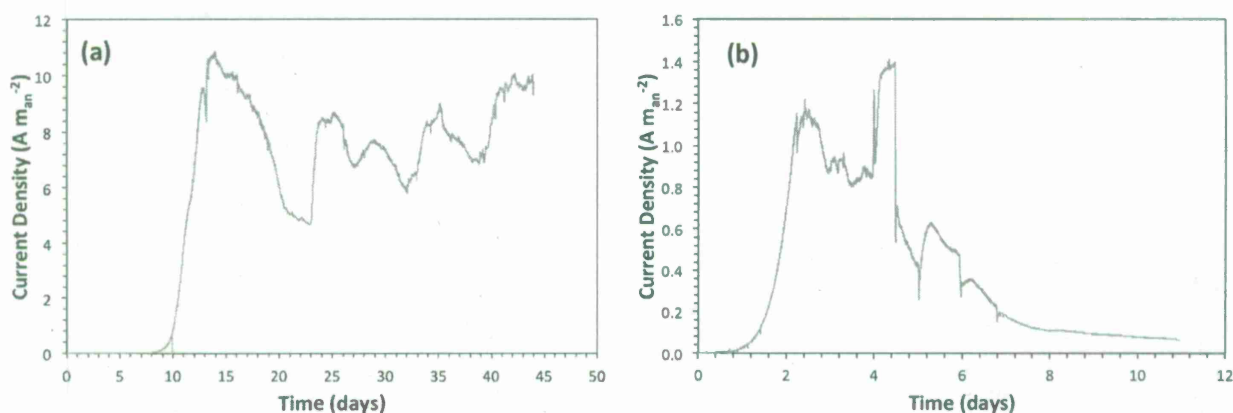


**Figure 1.1.** Performance of acetate-fed MECs with (a) a graphite rod anode and (b) a stainless steel mesh anode. The anode potential was poised at  $-0.4 \text{ V vs. Ag/AgCl}$ . The graphite rod anode MEC was operated in batch mode until day 22 and then continuously fed for the rest of the duration. The MEC with the stainless steel anode was operated in batch mode through the reported duration of operation. Note the different scales on the vertical axes.

We postulated that the stainless steel surface hindered the enrichment for ARB efficient in extracellular electron transport (EET) using a conductive biofilm matrix. We thus conducted cyclic voltammetry (CV) scans on one set of graphite rod and stainless steel mesh anode MECs to compare the possible EET mechanisms between the two. These CV scans are shown in Figure 1.2. The curve for the graphite rod anode MEC (Figure 2.2 (a)) fits the Nernst-Monod



model (fitting not shown) (Marcus et al., 2007; Torres et al., 2008b). This successful model fit, in combination with the high current densities, confirms the use of a conductive biofilm matrix for EET. The  $E_{KA}$  value determined from the curve fitting was -0.43 V vs. Ag/AgCl; this is consistent with values determined for *Geobacter* sp. (Torres et al., 2008b).

Contrastingly, the curve for the MEC with the stainless steel mesh anode (Figure 2.2 (b)) did not fit the Nernst-Monod model, even when using an enriched inoculum. We believe that stainless steel may have induced a change in the EET mechanism. It is known that OmcZ, an outer membrane cytochrome in *Geobacter* spp. is required for efficient EET and optimal current generation (Inoue et al., 2011). We suspect that stainless steel inhibited the functioning of this cytochrome, either due to its inherent chemical properties or leaching of metal ions, such as nickel and chromium that could have interacted negatively with important proteins. We are interested in continuing to evaluate the performance of stainless steel anodes to gain further insight into the reasons for the poorer performance of ARB. However, given the short timeline of the project, we moved forward with the use of graphite fibers as anodes for the MFC modules.

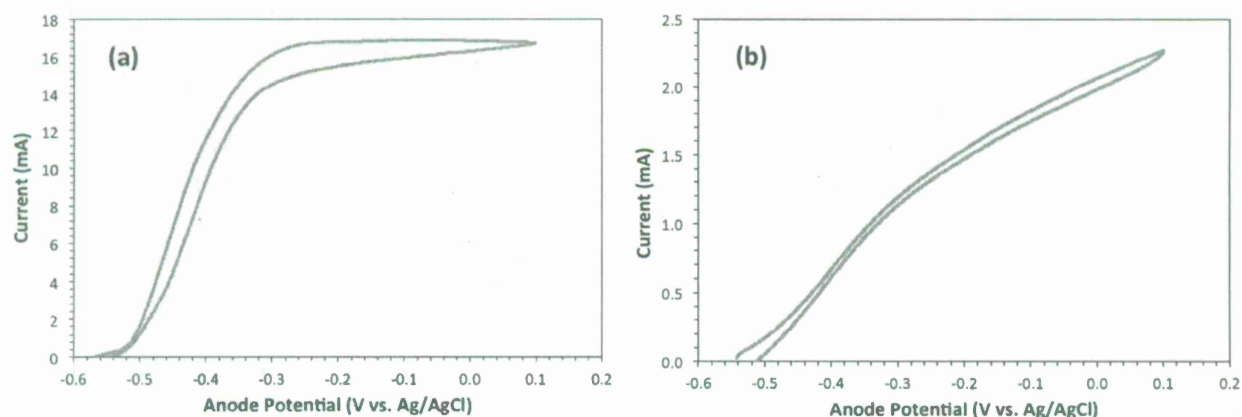


**Figure 1.2.** CV scans of acetate-fed MECs with (a) graphite rod anode and (b) stainless steel anode, performed after pseudo steady state. The scan rate was  $1 \text{ mV s}^{-1}$ . Note the different scales on the vertical axes.

## 2. Characterization and selection of anion exchange membrane:

The ion exchange membrane serves two purposes in an MFC. The first is to avoid crossover of  $\text{O}_2$  from the cathode chamber to the anode chamber, where anaerobic conditions need to be maintained for optimum growth and activity of efficient ARB. Avoiding  $\text{O}_2$  crossover also avoids



the growth of aerobic heterotrophic bacteria that would decrease the Coulombic efficiency by diverting electrons present in the substrate towards the reduction of  $O_2$ . The second is to allow efficient and preferential transport of ions from the anode chamber to the cathode chamber, or *vice versa*, to maintain electroneutrality.

It has been shown in the past that using a proton exchange membrane (PEM), which needs to transport  $H^+$  produced from anode respiration to the cathode chamber, leads to the development of pH gradients between the anode and the cathode chambers, with the cathode chamber pH shown often to reach close to 13 (Rozendal et al., 2007). From the Nernst equation, it is known that every pH unit that the cathode pH is higher than the anode pH leads to a loss of  $\sim 60$  mV of thermodynamic potential at room temperature. The underlying reason for this pH imbalance is that the anode chamber contains other cations such as  $Na^+$  and  $K^+$ , which are present in such high concentrations (10-100 mM) in comparison to  $H^+$  ( $\sim 10^{-4}$  mM), that electroneutrality is maintained through transport of these ions instead of  $H^+$ .

Researchers have investigated the use of other membranes, such as anion exchange membranes (AEMs) (Torres et al., 2008c), bipolar membranes (Ter Heijne et al., 2006), and simple filters/insulators (Kim et al., 2007), to avoid the issue of pH imbalance between the anode and the cathode chambers. Of these, AEMs have been found to perform well (Harnisch et al., 2008; Sleutels et al., 2009). When using an AEM to separate the anode and the cathode, electroneutrality is maintained by transport of  $OH^-$  from the cathode chamber to the anode chamber, either directly or via anionic buffers such as phosphate and carbonate species. The use of AEMs has consistently shown to reduce the pH imbalance between the anode and the cathode chambers in various MXCs, and we thus decided to use AEMs in developing our MFC prototypes.

While the use of AEMs to transport  $OH^-$  from the cathode chamber to the anode chamber has been proposed since 2007, a systematic study of various commercially available AEMs, in terms of their resistance to ion transport in conditions relevant to MFCs, has not been performed. Thus, we used electrochemical impedance spectroscopy (EIS) to characterize five commercially available AEMs (Table 2.1) in this aspect. For these experiments, we used electrochemical cells containing two chambers filled with relevant solutions (individually 100 mM PBS and 100 mM  $NaHCO_3$ ), with stainless steel rod electrodes, and separated by the membrane to be characterized. We performed EIS on the cell with one stainless steel rod as the working electrode, the other as the counter and reference electrode, and at 200 MHz and amplitude of 0.02 V. This allowed measurement of the Ohmic loss between the two electrodes for various membranes. We also performed EIS analysis without a membrane to get the background

Ohmic loss from the liquid solutions used, thus making it possible to determine the resistance to ion transport only from the membrane.

**Table 2.1.** List of membranes tested, including their supplier and physical properties.

Membrane	Supplier	Thickness	pH Stability
AMI-7001	Membranes International, USA	0.50-0.51	1-10
Excellion I-200	SnowPure, USA	0.32-0.34	NR
Fumasep FAA	FuMa-Tech, Germany	0.13-0.15	6-13
Fumasep FAB	FuMa-Tech, Germany	0.10-0.13	0-14
A201	Tokuyama, Japan	0.028	0-14

We show in Figure 2.1 the resistances to ion transport from different membranes in 100 mM PBS (Figure 2.1 (a)) and 100 mM  $\text{NaHCO}_3$  (Figure 2.1 (b)). AMI-7001 is a standard AEM that is used in various laboratory MXC studies (Parameswaran et al., 2009). We found that, of all the membranes we tested, AMI-7001 had among the largest resistances to transport of anions. The FAA, FAB, and A201 membranes provided significantly less resistance to anion transport compared to the AMI-7001 and I-200 membranes.

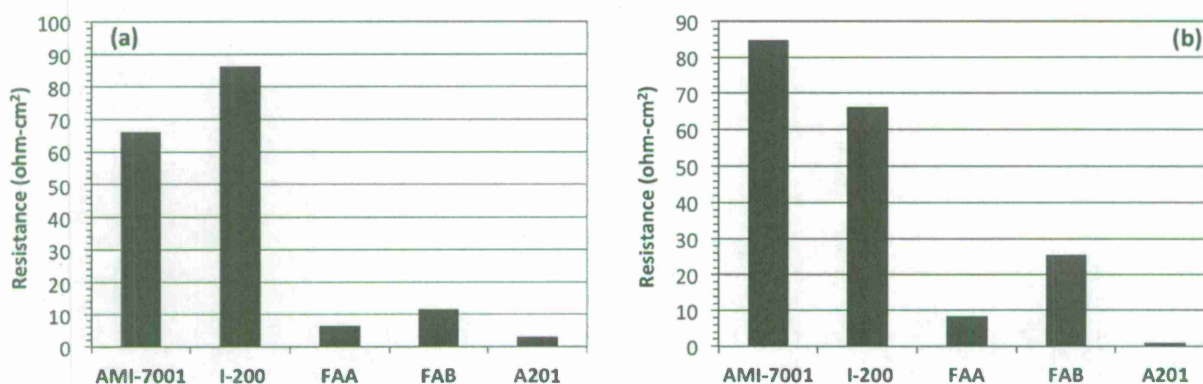


**Figure 2.1.** Resistances of various membranes tested in (a) 100 mM PBS, and (b) 100 mM  $\text{NaHCO}_3$ .

We selected A201 as the membrane to use in the MFC prototypes, since it provided the least resistance to anion transport irrespective of the electrolyte. Since A201 also has a much wider range of pH stability compared to AMI-7001, we anticipated that A201 also would be more stable over long-term operation.

### **3. Construction and performance of first MFC prototype:**

Based on the materials tested (described in sections 1 and 2) and the concepts from fuel cell designs, such as minimizing the distance between the anode and the cathode, we constructed our first flat-plate MFC prototype (Figure 3.1). Here we describe the salient features of our design. For the cathode, we decided to follow the guidelines that have been developed for construction cathodes for PEM fuel cells. The cathode design begins with a serpentine flow field (Figure 3.1 (a)), which is constructed from a graphite block that also acts as a current collector. This flow field allows efficient transport of  $O_2$  to the active cathode catalyst sites. It also allows removal of excess moisture that may be present on the cathode. While we conducted some experiments described below using this serpentine flow field, including the performance of the MFC we report below, we later discovered that the flow field was not essential in maintaining cathode performance. The flow rate of  $O_2$  in the flow field hardly affected the current densities, and an open-air cathode typically achieved the same current densities. Thus, the use of this serpentine flow field could be excluded while scaling up our design. However, this would require the use of an efficient current collector. In the laboratory, a stainless steel plate contacting the cathode at its edges (photo not shown) sufficed, but for larger systems, concepts such as building the cathode around a stainless steel mesh developed by Zhang et al. (2010) appear promising.

Next we describe the cathode itself, which is shown in Figure 3.1 (b). The cathode consists of a carbon cloth support. On one side of the cloth, which faces the serpentine flow field or is open to air, a paste of carbon and a hydrophobic polymer (in our case polydimethylsiloxane, or PDMS) is applied. The cloth together with this hydrophobic carbon layer is referred to as a gas diffusion layer (GDL). The GDL allows efficient transport of  $O_2$  to the catalyst sites by ensuring that  $O_2$  diffusion is not limited by "flooding" of the cathode. On the other side of the cloth, which faces towards inside the reactor, the catalyst layer is coated. We used Pt/C as the catalyst, at loadings of  $0.5 \text{ mg Pt/cm}^2$ . The Pt/C powder is mixed with an ionomer to form a paste, which is used to paint the catalyst later on the cloth. The ionomer allows transport ions,



thus maintaining charge neutrality. We used Nafion as the ionomer in the first set of designs we describe here, but evaluated its use critically later on (see section 5).

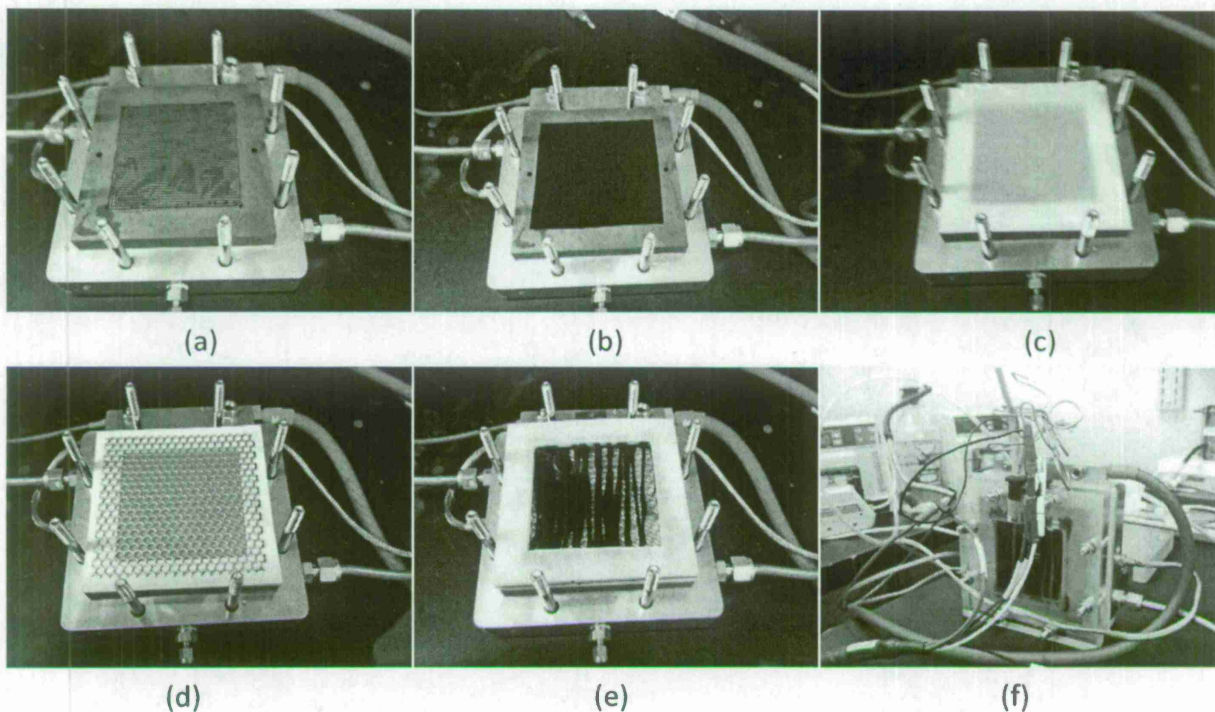


**Figure 3.1.** Photographs of the first flat-plate MFC prototype we developed at various stages of construction. See the text for details.

From the studies described in section 2, we selected A201 as the AEM of choice in the MFC design. The membrane is placed immediately next to the cathode (Figure 3.1 (c)) to minimize distance between the anode and the cathode. On the side of the membrane opposite to the one facing the cathode, we placed a stainless steel mesh (Figure 3.1 (d)). In other studies that we have done with various MFC designs, we had noted that the flow of anions from the cathode to the anode chamber causes the membrane to deform, bending towards the anode side. This deformation leads to increased Ohmic losses. Others also have seen this phenomenon (Zhang et al., 2010). We thus used the mesh to support the membrane against the cathode in order to prevent membrane deformation. In subsequent trials (not reported here), we replaced the stainless steel mesh with a plastic mesh to avoid corrosion.

After the mesh to support the membrane, we placed the anode, which consisted of a titanium frame acting as a current collector, with wound carbon fibers to allow enough anode area for ARB to grow (Figure 3.1(e)). The anode chamber was then closed with a Plexiglas frame. A photograph of the final set-up is shown in Figure 3.1 (f). In our prototypes, we used an anode

volume of 100 mL, but this can be easily adjusted to achieve required rates of power production.

We conducted three trials using this design, replacing certain elements (e.g., the mesh material to support the membrane) in each iteration. We report here results from only one of the trials. In all trials, we used acetate as the electron donor for ARB and inoculated the MFCs with a *Geobacter* sp.-enriched inoculum from other operating reactors in our laboratory. We used a phosphate-buffered medium for growing ARB, which has a conductivity of 15.5 mS/cm. We started all MFCs in batch-mode, and switched them to continuous mode once we observed current production, at a hydraulic retention time of 4-6 hours. We operated all MFCs with a potentiostat, with the anode potential poised at -0.3 V vs. Ag/AgCl. We continuously monitored the current production, as well as the cathode potential, to determine power densities. We show in Figure 3.2 below, the performance of one of the prototypes we constructed.

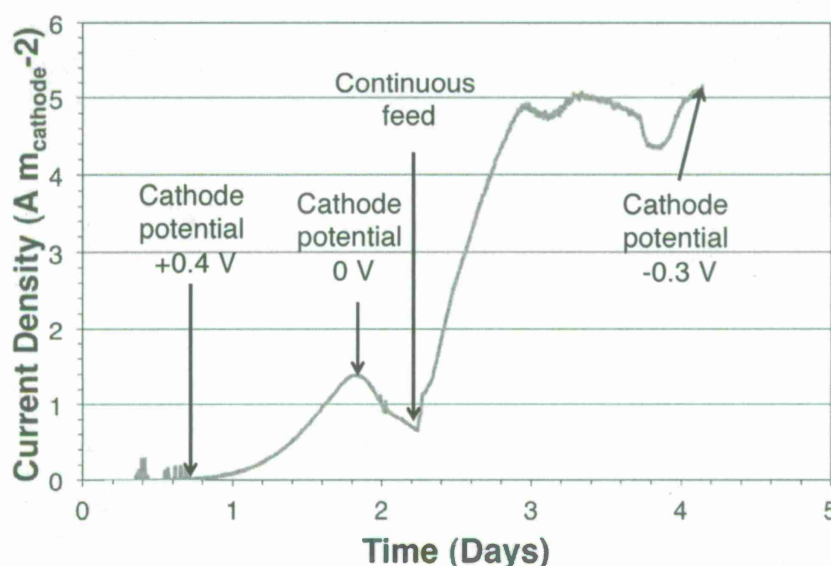


**Figure 3.2.** Performance of one of our MFC prototypes in terms of current density vs. time.

Using an active inoculum, we observed current production within one day of starting the MFC. The cathode open circuit potential (OCP, i.e., when current production had not begun) was +0.4 V vs. Ag/AgCl. This is lower than the expected theoretical OCP for oxygen reduction of +0.54 V vs. Ag/AgCl (or +0.81 V vs. SHE). In other trials, the OCP was as low as ~+0.15 V vs. Ag/AgCl, suggesting that roughly 0.2-0.4 V of theoretically available voltage was lost even without any current production, possibly due to mixed potential arising from possible side reactions. The current density increased with time up to ~1.5 A/m<sub>cathode</sub><sup>2</sup>, after which there was a decrease



due to consumption of all acetate, since the anode volume was very small. We switched the MFC to continuous mode thereafter, and the current density increased to up to  $5 \text{ A/m}^2$ .

The continuous measurement of the cathode potential showed that, by  $1.5 \text{ A/m}^2$ , the cathode potential had already decreased to  $0 \text{ V vs. Ag/AgCl}$ . This represents a power density of  $\sim 450 \text{ mW/m}^2$ . The maximum power density was achieved at a current density of  $\sim 4 \text{ A/m}^2$ , when the cathode potential was  $\sim -0.1 \text{ V vs. Ag/AgCl}$ , which amounts to a power density of  $\sim 800 \text{ mW/m}^2$ . These power densities are on the lower end of what has been observed in laboratory studies in the past 3-4 years in ours (Torres et al., 2008c), as well as other groups (Logan et al., 2008). By  $5 \text{ A/m}^2$ , the cathode potential reached  $-0.3 \text{ V vs. Ag/AgCl}$ , at which point no power was being produced. Since the anode potential was set at  $-0.3 \text{ V vs. Ag/AgCl}$ , only  $\sim 0.25 \text{ V}$  was lost to anode potential losses (anode OCP should be  $\sim -0.55 \text{ V vs. Ag/AgCl}$ ) at the highest current densities, while  $\sim 0.85 \text{ V}$  was lost at the cathode. Note that this also includes the Ohmic loss, which we estimate to be  $< 0.1 \text{ V}$ , unless ionic contact between the membrane and the cathode was poor. This tells us that the power densities in our MFC design were limited by the cathode reaction. Although this was surprising, since Pt/C catalyst allows obtaining current densities that are 100-1000 times higher in chemical fuel cells, we acknowledged that cathodic limitations have been increasingly determined as a key parameter in scaling up MFCs based on various other studies in the last few years (Cheng and Logan, 2006; Rismani-Yazdi et al., 2007; Fan et al., 2007). Thus, we decided to focus on understanding the MFC cathodic limitations in more detail (Section 5). We believe that solving cathodic limitations will be an important step in gearing MFCs towards scale-up and practical applications.

#### **4. Characterization of anode and Ohmic losses in MECs:**

Before conducting studies on the cathode, we determined the anode and Ohmic losses in our design. To do this, we conducted further studies in microbial electrolysis cells (MECs). In MECs,  $\text{O}_2$  is excluded from the cathode, and instead water is reduced to  $\text{H}_2$  gas. The absence of  $\text{O}_2$  at the cathode is advantageous to characterize the anode, in which ARB could be inhibited by the  $\text{O}_2$  diffused from the cathode. This configuration requires  $\sim 0.14 \text{ V}$  of energy input to make the  $\text{H}_2$ -evolution reaction on the cathode thermodynamically favorable. In reality, additional voltage needs to be applied to overcome potential losses at the anode, at the cathode, and due to ion transport (i.e., Ohmic losses). By tracking the applied voltage as a function of current density and using various electrochemical techniques, we could separate the contribution of each to the total applied voltage. For these studies, we used an MEC that included the same anode and membrane we used in our MFC prototypes (see Figure 4.1 for photograph of MEC),



as well as the same design features (for e.g. short distance, i.e. <0.5 cm, between the anode and the cathode).

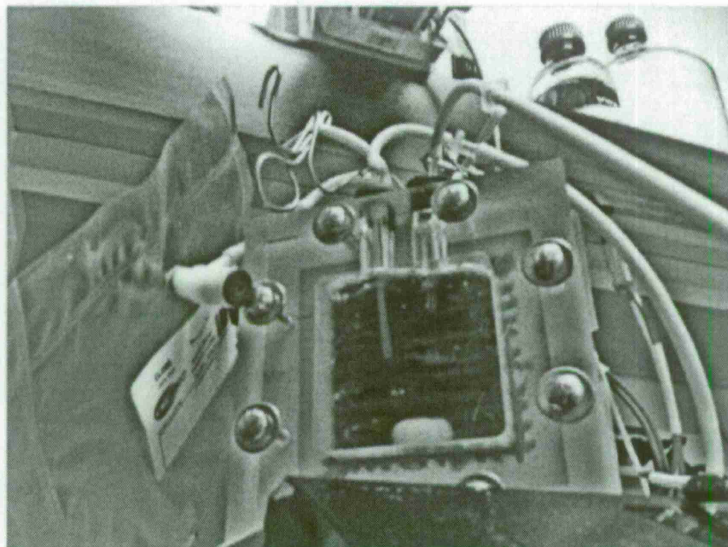


**Figure 4.1.** Photograph of MEC used to study anode and Ohmic losses for our electrode configuration.

In the flat-plate MEC, we were able to achieve volumetric current densities of up to 500 A/m<sub>anode</sub><sup>3</sup>. Note that we use the current density normalized to anode volume in the discussion here, as opposed to that normalized to cathode area, since with improving the anode performance and reducing Ohmic losses, the primary aim is to obtain high anodic volumetric current densities. Once the ARB biofilm had fully grown and a steady-state current density was reached, we performed cyclic voltammetry (CV) on the biofilm to get insights into anode potential losses. We show the CV below in Figure 4.2. The CVs showed typical Nernst-Monod behavior of ARB kinetics, with the maximum current densities achieved by an anode potential of -0.35 V vs. Ag/AgCl. This represents an anode potential loss of only 0.2 V, which agrees with our previous studies described in this report. The maximum volumetric current density we report here also is among the highest reported, confirming that using a large surface area anode allowed reaching high current densities, while minimizing additional potential losses.

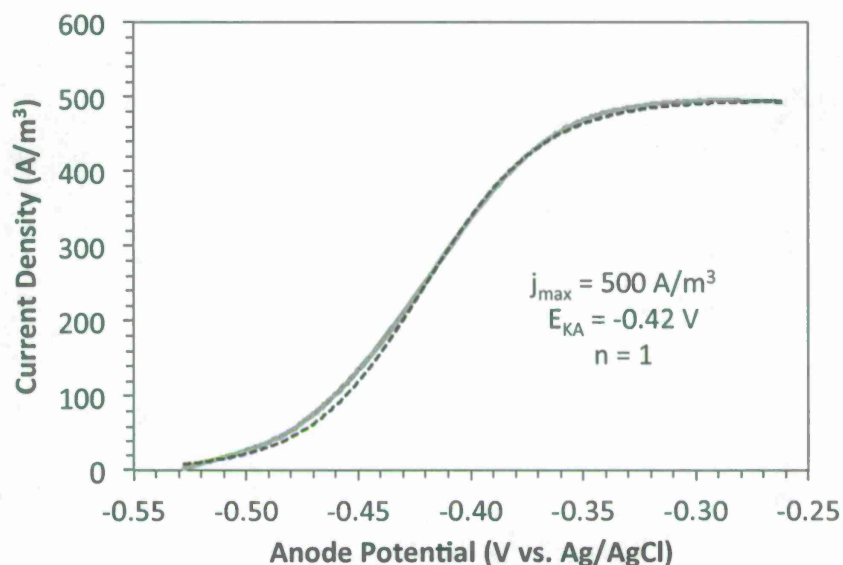


**Figure 4.2.** Cyclic voltammetry of MEC ARB biofilm.

We further characterized MEC performance by using additional electrochemical techniques. First we performed EIS analysis at open circuit to determine the Ohmic loss. It was negligible, since our design places the anode and the cathode <0.5 cm apart and also because we used a relatively high conductivity phosphate buffer on the anode chamber. We then performed chronoamperometry, changing the anode potential from open circuit to -0.3 V vs. Ag/AgCl, while recording current density, cathode potential, and cathode liquid pH. We then used this information to separate the various components of applied voltage, and these are shown in Figure 4.3. We show that anode and Ohmic potential losses contribute together only a small fraction of the total applied voltage (or potential losses). Although we separate pH losses from cathode losses in Figure 4.3, we show in section 5 that these are typically also associated with the cathode, and thus even in MECs, we conclude that cathode losses result in the highest fraction of applied voltages at a given current density. Thus, EIS confirms that our design helps ensure that anode and Ohmic potential losses are minimized. It also confirms the importance of finding ways in which we can improve cathode performance.

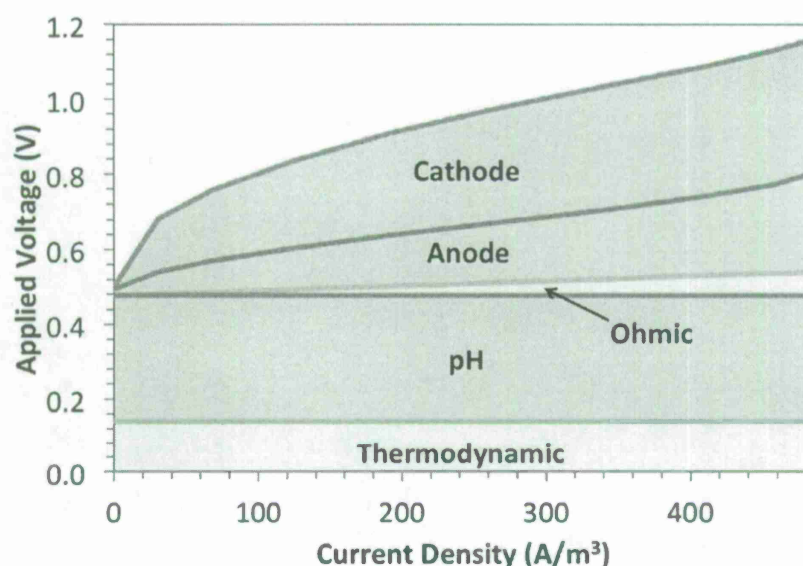


Figure 4.3. Applied potential as a function of current density in the MEC.

### 5. Identification and characterization of cathodic overpotentials\*

Because our first prototype MFC was limited by cathode performance, we decided to investigate the reasons for this limitation. In general, it has become evident over the last few years that MFCs are more likely to be limited, in terms of maximum achievable power densities, by cathodic potential losses (Zhao et al., 2006; Rozendal et al., 2008; Rismani-Yazdi et al., 2008). Our aim was thus to understand the underlying reasons for cathodic potential losses at typical current densities ( $0\text{--}20\text{ A/m}_{\text{cathode}}^2$ ) and, as a direct outcome, evaluate solutions to overcome these losses.

It is often suggested that cathodes in MFCs are limited because of the difficulty providing protons, a supposed reactant at the active catalyst sites, at typical conditions, such as neutral pH. This assumes that the oxygen reduction reaction (ORR) proceeds as follows, based on proton exchange membrane (PEM) fuel cells:



However, cathodes in MFCs are subjected to significantly different conditions than in PEM fuel cells, e.g., direct contact with an electrolyte at neutral pH. Thus, we first analysed whether this

\* The work described in this section led to the publication: S. C. Popat, D. Ki, B. E. Rittmann, C. I. Torres (2012). Importance of  $\text{OH}^-$  transport from cathodes in microbial fuel cells. *ChemSusChem*, 5, 1071-1079.



minimal availability of protons as reactant can actually support the cathodic current densities typically observed in MFCs.

If the ORR proceeds on cathodes in MFCs through the use of protons as a reactant, the flux of protons through the catalyst layer and the diffusion boundary layer, of the cathode, has to be sufficient enough to support the current densities of  $5\text{--}10\text{ A/m}^2$  that are usually observed. This transport of protons occurs mainly through diffusion. Using typical values for the diffusion boundary layer thickness, we computed a maximum flux of protons in the order of  $10^{-10}\text{--}10^{-9}\text{ mmol/cm}^2\cdot\text{s}$ , which corresponds to current densities in the order of  $10^{-3}\text{--}10^{-2}\text{ A/m}^2$ . This is 100-1000 times lower than current densities typically observed; thus, we conclude that ORR does not proceed in MFCs as it does in PEM fuel cells. It must occur through the alternative mechanism, shown below, which is dominant in alkaline fuel cells (Varcoe et al., 2005):



We hypothesized that cathodes in MFCs are limited because of poor  $\text{OH}^-$  transport out of the cathode into the bulk electrolyte. Inability to rapidly transport  $\text{OH}^-$  from the active catalyst sites to the bulk liquid will result in an increase its local concentration, leading to concentration over-potential. From the Nernst equation, every increase in one pH unit decreases the redox potential for the ORR by  $\sim 59\text{ mV}$  (at room temperature), and thus we postulated that a significant amount of cathodic potential loss at typical current densities is likely associated with an increase in the local cathode pH.

The first reason for this limitation stems from the anion-conduction properties of the catalyst binder used for creating a three-phase boundary for the ORR. As an extrapolation from its use in PEM fuel cells, Nafion has been the binder of choice in cathodes in many MFCs (Cheng et al., 2006). However, Nafion contains sulfonate moieties that are efficient in transporting cations, but provide significant resistance to transport of anions, including  $\text{OH}^-$  (Piela et al., 2006). Buffers, such as phosphate and carbonate species, that would help transport  $\text{OH}^-$  out of the cathode would also be transport-limited in Nafion. Second is the lack of sufficient agitation, which results in a thicker diffusion boundary layer.

We decided to confirm that  $\text{OH}^-$  transport limits cathode performance. For this, we obtained a series of cathode polarization curves under different conditions in a gas-diffusion half-cell. We prepared cathodes ( $9\text{ cm}^2$ ) from 30% wet-proofed carbon cloth gas-diffusion boundary layers coated with a microporous carbon layer (CMPL) on one side (Electrochem Inc., USA). We prepared catalyst ink using 0.5 g of 30% Pt/C powder (Electrochem Inc., USA) mixed in 5 mL of 5% ionomer in iso-propanol solution (Nafion, Sigma-Aldrich, USA, or AS-4, Tokuyama

Corporation, Japan) by sonication for 30 minutes and magnetic stirring for 24 h, as binder, and applied it the side of cathodes opposite to the CMPL, using a paint brush. We used a Pt loading of  $0.5 \text{ mg/cm}^2$  on all the cathodes. We constructed gas-diffusion half-cells ( $3 \text{ cm} \times 1.8 \text{ cm} \times 3 \text{ cm}$ ) as Plexiglas chambers of  $\sim 16 \text{ mL}$  volume, closed at one end. We placed the cathodes at the other end with the catalyst-coated side facing inside (towards the solution) and the MPCL outside (towards air). We used a saturated calomel electrode ( $+0.244 \text{ V}$  vs. SHE) as the reference electrode and placed it inside the cells at a distance of  $5 \text{ mm}$  from the cathode. We used a stainless steel rod as the counter electrode ( $\sim 9 \text{ cm}^2$ ,  $5 \text{ mm}$  diameter). We performed linear sweep voltammetry (LSV) on cathodes at  $30^\circ\text{C}$  using a potentiostat (Princeton Applied Research, USA) at a scan rate of  $1 \text{ mV/s}$ . We performed i-R correction for all LSVs to correct for the Ohmic loss between the reference electrode and the cathode, using an average Ohmic loss as measured from  $\sim 20$  impedance spectroscopy measurements at  $100 \text{ kHz}$  with an amplitude of  $10 \text{ mV}$ .

We first obtained polarization curves for cathodes constructed with Nafion binder in unbuffered  $100 \text{ mM NaClO}_4$  solution at pH 7.5, 10.8, or 13 (Figure 5.1 (a)). It is evident that the cathode in pH 7.5 had the largest potential losses, particularly at low current densities. The difference in potential for the cathode in pH 7.5 vs. the cathodes in higher pH was only maintained at current densities  $< 1 \text{ A/m}^2$ , indicative of high potential losses at low current densities. These losses also decreased with increasing bulk liquid pH, indicating that they are related directly to the concentration gradient for  $\text{OH}^-$  between the bulk liquid and the cathode. Eventually, all cathodes converged to the same potential at high current densities, suggesting that all of them reach the same local pH, irrespective of the bulk liquid pH. This experiment provides the first indication of the importance of  $\text{OH}^-$  transport from cathodes. Using the polarization curve for the cathode in pH 13, we determined  $j_0$  (i.e., the exchange current density) and  $\alpha$  (i.e., the charge transfer coefficient), both values being related to catalyst properties, as  $9.5 \times 10^{-8} \text{ A/cm}^2$  and 0.195, respectively. Next, we used the Butler-Volmer equation with the  $j_0$  and  $\alpha$  values to predict the response of the cathode in pH 7.5 if it were not  $\text{OH}^-$  transport limited. We show this in Figure 5.1(b). It is evident that the actual response includes additional overpotential, which has to be related to  $\text{OH}^-$  transport limitations. We also fit the experimental curve to the Butler-Volmer equation that includes diffusion limitation to obtain the local cathode pH as a function of the current density, which increased to  $> 11$  very rapidly at current densities  $< 1 \text{ A/m}^2$  and at  $10 \text{ A/m}^2$  was  $> 12.5$ . This represents a potential loss of  $> 300 \text{ mV}$ , or  $> 50\%$  of all cathodic potential losses typically observed in this range of current density.

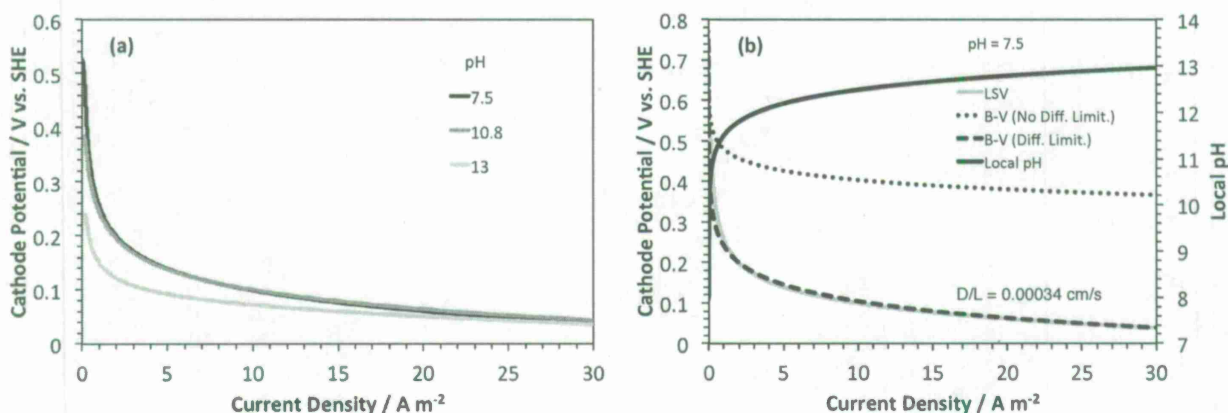


**Figure 5.1.** (a) Polarization curves of Pt-based gas diffusion cathodes constructed with Nafion binder in 100 mM NaClO<sub>4</sub> solution at different pH. (b) Comparison of polarization curve of Pt-based gas diffusion cathode constructed with Nafion binder in 100 mM NaClO<sub>4</sub> solution at pH 7.5 with curves predicted from the Butler-Volmer equation without and with OH<sup>-</sup> diffusion limitation, and the predicted local cathode pH as a function of current density resulting from OH<sup>-</sup> diffusion limitation.

While the above experiments were performed in unbuffered solutions, a buffer is typically used in MFCs to maintain the bulk liquid pH closer to neutral. This buffer could also help in transporting OH<sup>-</sup> from the cathode to the bulk liquid. Thus, we obtained polarization curves for cathodes constructed with Nafion binder in 100-mM phosphate buffer. Similar to the above experiments, we performed these experiments in buffer solutions with different pH, ranging from 7.2 to 12.9, but we show only the polarization curve in pH 7.2 in Figure 5.2. We also compare the experimentally obtained polarization curve of the cathode in pH 7.2 with the theoretical non-diffusion controlled response in pH 7.2, as determined from the Butler-Volmer equation. The difference between the two provides a measure of potential losses related to increased local cathode pH. At a current density of 10 A/m<sup>2</sup>, this difference was >0.3 V, suggesting that the local cathode pH was already ~5 units higher than the bulk liquid pH. Potential losses related to OH<sup>-</sup> transport limitation were smaller at low current densities (<5 A/m<sup>2</sup>), but still represented a significant fraction. For example, potential loss related to OH<sup>-</sup> transport limitation was ~0.15 V at 4 A/m<sup>2</sup>, corresponding to a local cathode pH of ~9.7. This pH represents the tail end of where a favourable concentration gradient could exist for OH<sup>-</sup> transport through deprotonation of H<sub>2</sub>PO<sub>4</sub><sup>-</sup> to HPO<sub>4</sub><sup>2-</sup>.



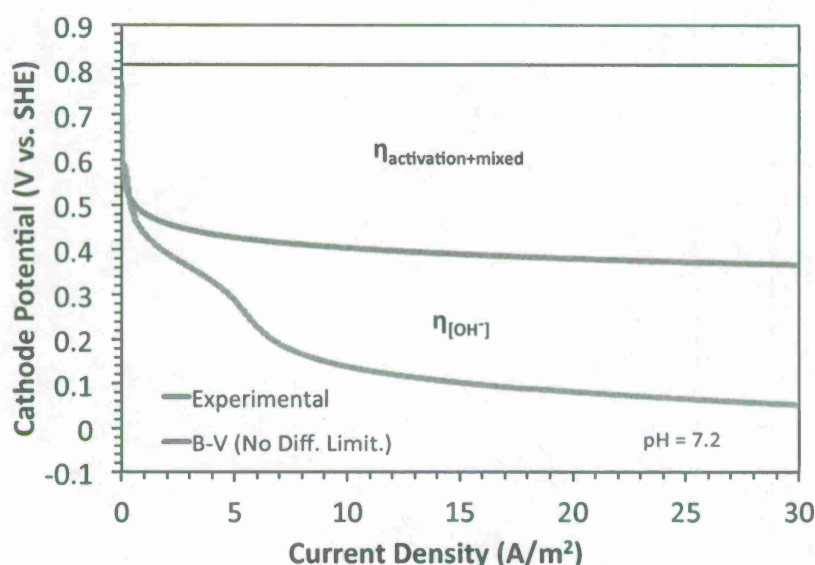


**Figure 5.2.** Comparison of polarization curve of Pt-based gas-diffusion cathode constructed with Nafion binder in 100 mM phosphate buffer at pH 7.2 with curves predicted from the Butler-Volmer equation without OH<sup>-</sup> diffusion limitation.

Having established that Nafion provides significant resistance to OH<sup>-</sup> transport, either directly or through phosphate buffer as OH<sup>-</sup> carrier, we hypothesized that replacing Nafion with an anion-conductive polymer will result in improved cathode performance. Several polymers containing quaternary ammonium moieties have good anion exchange capacity and are available from applications in anion exchange membrane (AEM) fuel cells (Varcoe et al., 2006; Fang et al., 2006; Xiong et al., 2008). We selected one of these, AS-4 (Tokuyama Corporation). We obtained polarization curves for cathodes constructed with AS-4 binder in 100-mM phosphate buffer at pH 7.2 and compared these to those for cathodes constructed with Nafion binder. We show this comparison in Figure 5.3. Compared to the cathodes with Nafion binder, potential losses for the cathode with AS-4 binder were lower. Since we expect activation-related overpotentials to be the same for both cathodes, the improved performance of the cathode with AS-4 binder is a direct result of improved OH<sup>-</sup> transport, either directly or through improved transport of the anion buffer species. Within the range of current densities typically observed in MFCs, potential losses for the cathode with AS-4 binder were up to 157 mV lower than for the cathode with Nafion binder, indicating significant improvement in anion transport. Considering this result, we suggest that the use of Nafion as the cathode catalyst binder in MFCs be replaced with anion conductive binders like the one we used here.

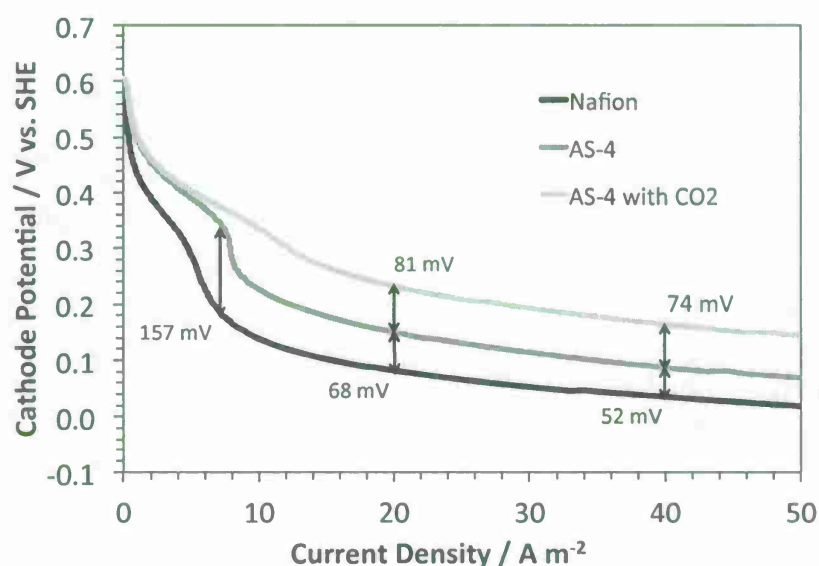


**Figure 5.3.** Comparison of polarization curves of Pt-based gas-diffusion cathode constructed with Nafion and AS-4 binders, the latter with and without CO<sub>2</sub> feed to the cathode, in 100 mM phosphate buffer at pH 7.2.

The maximum savings of 157 mV at 7.5 A/m<sup>2</sup> suggests that the local cathode pH was ~2.6 units lower with the AS-4 binder. Since the cathode with the Nafion binder was close to a local pH 12 at this current density (as we determined previously), the local cathode pH with AS-4 binder was ~9.4. This still represents a significant remaining potential loss related to OH<sup>-</sup> transport (~140 mV) and, thus, additional opportunity for improving cathode performance.

A second way to improve cathode performance would be through providing additional buffer in the form of CO<sub>2</sub>. We have shown in the past that adding CO<sub>2</sub> to the cathode chamber in MFCs containing a membrane helps in transporting OH<sup>-</sup> across the membrane (Torres et al., 2008c). H<sub>2</sub>CO<sub>3</sub> (hydrated CO<sub>2</sub>) would deprotonate to HCO<sub>3</sub><sup>-</sup>, thus acting as an OH<sup>-</sup> carrier. The advantage of providing CO<sub>2</sub>, especially to gas-diffusion cathodes, is that it can be delivered directly to the catalyst sites through the gas diffusion boundary layer, compared to phosphate buffer that suffers from the same diffusion limitations as OH<sup>-</sup>. Also, the second pK<sub>a</sub> of the CO<sub>2</sub> buffer system is 10.3, and this would allow maintaining a lower cathode pH at high current densities than phosphate, through OH<sup>-</sup> transport via the HCO<sub>3</sub><sup>-</sup>/CO<sub>3</sub><sup>2-</sup> couple.

We obtained polarization curves for the cathodes constructed with AS-4 binder with CO<sub>2</sub> feed (5% mixture with air) as well (Figure 5.3). It is apparent that CO<sub>2</sub> addition did not significantly help in the region of low current density (< 5 A/m<sup>2</sup>), since phosphate already was partially aiding OH<sup>-</sup> transport. However, CO<sub>2</sub> addition resulted in lower potential losses at the higher

current densities. Compared to the cathode with Nafion (and no  $\text{CO}_2$ ), potential losses were  $\sim 120\text{--}140$  mV lower for the cathode with AS-4 with  $\text{CO}_2$  addition, thus representing a local cathode pH close to 10. We thus conclude that enhanced  $\text{OH}^-$  transport was occurring through the deprotonation of  $\text{H}_2\text{CO}_3$  to  $\text{CO}_3^{2-}$ .

Since we found that the cathode performance depended primarily on the  $\text{pK}_a$  of the buffer used, we explored the use of ammonium ( $\text{NH}_4^+$ ) as a sustainable buffer for improving cathode performance in MFCs. While this might not be a practical application for the purposes of developing a microbial power generator for naval bases, the use of  $\text{NH}_4^+$  as buffer could be feasible for treatment of waste streams already containing high  $\text{NH}_4^+$  concentrations. The  $\text{NH}_4^+/\text{NH}_3$  couple has a  $\text{pK}_a$  of  $\sim 9.2$ , suggesting that it should be possible to maintain the local cathode pH in MFCs in the range of 8.5–10 using  $\text{NH}_4^+$  as a buffer, thus further reducing potential losses. To compare the performance of cathodes in  $\text{NH}_4^+$  buffer against other buffers, we obtained polarization curves for cathodes constructed with Nafion binder in 50 mM of various solutions (Figure 5.4). As expected, the cathode overpotential in 50-mM unbuffered solutions (NaCl) increased rapidly, even at low current densities, as a result of an increase in the local cathode pH. Our previous analysis suggests that, by  $2 \text{ A m}^{-2}$ , the local cathode pH already increases by 4–5 pH units in the absence of a buffer, thus representing a significant Nernstian concentration overpotential of  $\sim 300$  mV due to local accumulation of  $\text{OH}^-$ . In contrast, the cathode overpotential to reach current densities of up to  $5 \text{ A m}^{-2}$  was lower in PBS. This was a result of buffering of pH in the range of 7.2–9, which represents the tail end of where  $\text{H}_2\text{PO}_4^-$  deprotonates with  $\text{OH}^-$ . Beyond this current density, the rate of production of  $\text{OH}^-$  surpassed the rate of transport of  $\text{H}_2\text{PO}_4^-$ , which encountered transport resistance in the catalyst layer due to the use of Nafion as the catalyst binder. Bicarbonate buffer did not significantly help in buffering close to the  $\text{pK}_a$  of the  $\text{HCO}_3^-/\text{CO}_3^{2-}$  couple of  $\sim 10.3$ , but this could be due to its poor transport properties in Nafion.

In comparison to phosphate and bicarbonate buffers, the overpotentials in  $\text{NH}_4\text{Cl}$  and  $\text{NH}_4\text{HCO}_3$  were lower at high current densities ( $>5 \text{ A m}^{-2}$ ). This confirms our hypothesis that  $\text{NH}_4^+$  helped to maintain a lower local cathode pH. Up until  $5 \text{ A m}^{-2}$ , the cathode in PBS performed better than in  $\text{NH}_4\text{Cl}$  and  $\text{NH}_4\text{HCO}_3$  because of the buffering effect of phosphate in the pH range of 7.2–9. However, current densities up to  $25 \text{ A m}^{-2}$  were sustained in  $\text{NH}_4^+$  solutions without the LSVs showing an inflection resulting from transport limitation. This likely was an effect of using Nafion as the catalyst binder, since Nafion is efficient in transporting cations, such as  $\text{NH}_4^+$ . We had shown before that replacing Nafion as the binder with an anionomer can help improve cathode performance when using phosphate or bicarbonate as buffer, but for  $\text{NH}_4^+$  buffer,



Nafion is a preferable binder. The higher diffusion coefficient for  $\text{NH}_4^+$ , compared to the other buffers, also increases its relative transport rates to the cathode surface.

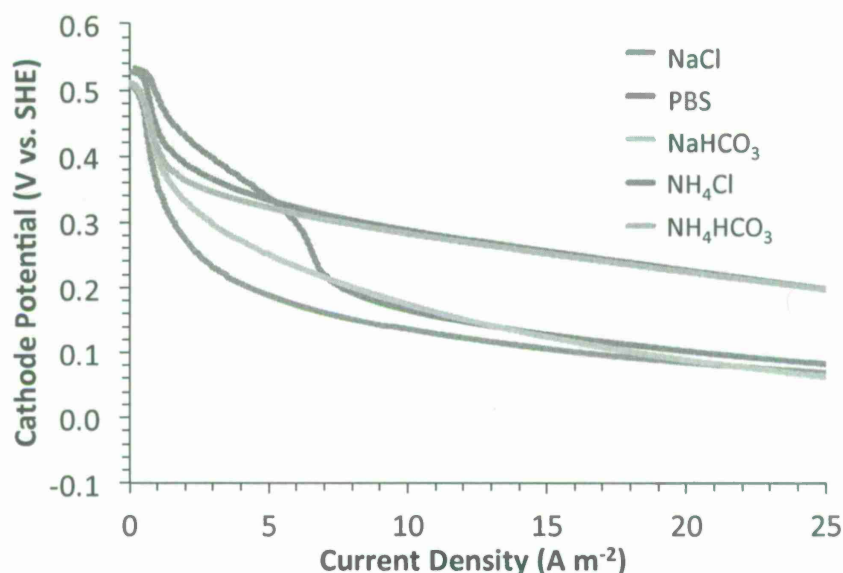


**Figure 5.4.** Polarization curves of Pt-based gas-diffusion cathodes in different 50-mM solutions.

The results in Figure 5.4 show that it is possible to save >150 mV at current densities >10  $\text{A m}^{-2}$  using  $\text{NH}_4^+$  as a buffer at the same concentrations as phosphate. This is an important result and has especially favorable implications for treatment of streams containing high levels of  $\text{NH}_4^+$ , such as animal waste. However, it has been shown in the past that  $\text{NH}_3$  can be lost through air-cathodes in MFCs following deprotonation of  $\text{NH}_4^+$ . Thus, any  $\text{NH}_3$  that partitions in the gas phase at the cathode should be recovered to sustainably use the buffer.

Next, we studied the importance of  $\text{NH}_4^+$  transport on cathode performance; we obtained polarization curves for cathodes constructed with Nafion binder in solutions of different concentrations of  $\text{NH}_4^+$ . These results are shown in Figure 5.5. The experiments confirm that cathode performance was directly related to  $\text{NH}_4^+$  concentration and, thus, its transport. Most notably, we saw the inflections in LSVs within the tested range of current densities that we observed earlier with 50-mM PBS, this time with 10- and 25-mM  $\text{NH}_4\text{Cl}$ . Beyond the current densities where the inflection was observed, the transport of  $\text{NH}_4^+$  was slower than the production of  $\text{OH}^-$ , and, logically, the inflection appeared at a lower current density for 10-mM  $\text{NH}_4\text{Cl}$  than for 25-mM  $\text{NH}_4\text{Cl}$ . At higher concentrations,  $\text{NH}_4^+$  transport was not limiting within the range of current densities tested. Therefore, we saw no inflection points for  $\text{NH}_4\text{Cl} \geq 50$  mM.

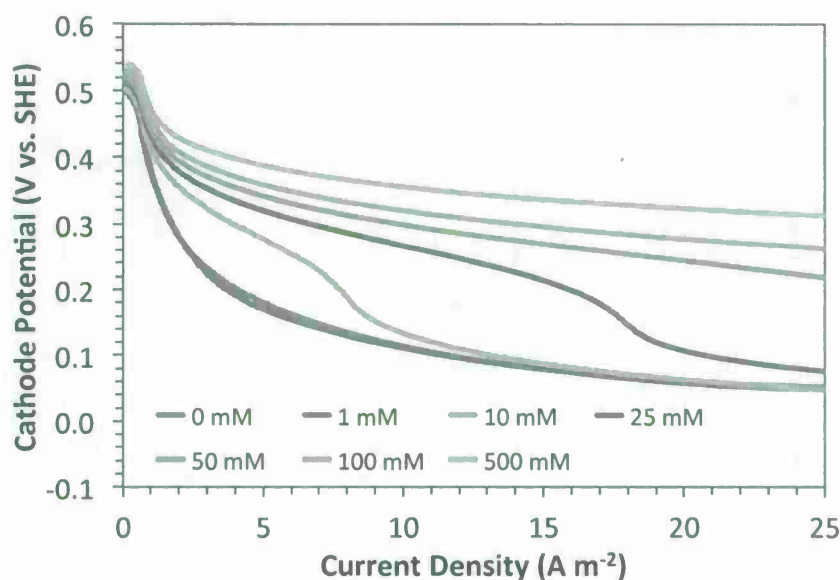


**Figure 5.5.** Polarization curves of Pt-based gas-diffusion cathodes in solutions containing different concentrations (0-500 mM)  $\text{NH}_4\text{Cl}$  with 25-mM  $\text{NaCl}$  as background.

## 6. Development of co-culture for enhanced energy recovery from sucrose:

One of our goals for this project was to achieve high current densities along with high Coulombic efficiencies when feeding sucrose as a substrate to MFCs. Since high current density producing ARB, such as *Geobacter* sp., can consume only simple substrates such as acetate, we developed a complementary mixed microbial culture that ferments sucrose primarily to acetate. We describe below our approach in developing such a homo-acetogenic culture, as well as its characterization in terms of electron recovery from sucrose as acetate and its community structure using molecular tools.

We set up a 0.5-L batch reactor fed with medium with the following composition (in 1 L):  $\text{KH}_2\text{PO}_4$  0.2 g;  $\text{NaCl}$  1 g;  $\text{NH}_4\text{Cl}$  0.5 g;  $\text{KCl}$  0.1 g;  $\text{MgCl}_2 \cdot 6\text{H}_2\text{O}$  0.25 g;  $\text{CaCl}_2 \cdot 2\text{H}_2\text{O}$  0.175 g; BES 6.02 g (for selective methanogenic inhibition),  $\text{NaHCO}_3$  4.2 g (50 mM); trace mineral media as published in Parameswaran et al (2009) 1mL; ATCC vitamins solution 0.5 mL,  $\text{Fe}^{2+}$  at 4 g/L 1 mL; and  $\text{Na}_2\text{S} \cdot 7\text{H}_2\text{O}$  at 37 g/L 0.1 mL. We added 10 mmoles of sucrose to the batch reactor (i.e., 20 mM concentration). The initial medium pH was stable at around 6.75. We had previously enriched a consortium of homo-acetogenic bacteria from the suspension of an H-type MEC that produced current from a syntrophic interaction between homo-acetogens and ARB (Parameswaran et al, 2011). We added 5 mL of the enrichment culture to serve as inoculum

(1% of reactor volume) to obtain enrichment on sucrose, as well as conducting a thorough electron balance.

Batch reactions proceeded immediately, leading to complete sucrose utilization by the second day (Figure 6.1). The reactor pH dropped to 6.05 on day 2, but quickly stabilized back to 6.5 after that time point, and it remained stable until the end of batch operation (day 7). Of the characterized soluble products at the end of the batch run, lactate was the dominant sink, followed by acetate. Formate is a precursor for homo-acetogenesis (Ha et al, 2008) and should be considered as a readily utilizable substrate when homo-acetogenesis is not limiting. Lactate, acetate, and formate constituted about 40% of the total electrons from sucrose at the end of the batch run.

After a week of batch operation, we shifted the reactor to semi-continuous mode along with an increase in buffer concentration to 100 mM bicarbonate and a decrease in sucrose influent concentration to 10 mM. Semi-continuous operation involved replacing 200 mL of the medium once a week. Corresponding to this change, the product distribution shifted to almost all acetate (~75% of the total electrons), along with some propionate (7% of total electrons) and the rest as biomass (Figure 6.1), after 23 days of semi-continuous operation. The pH in the reactor remained steady at around 7.

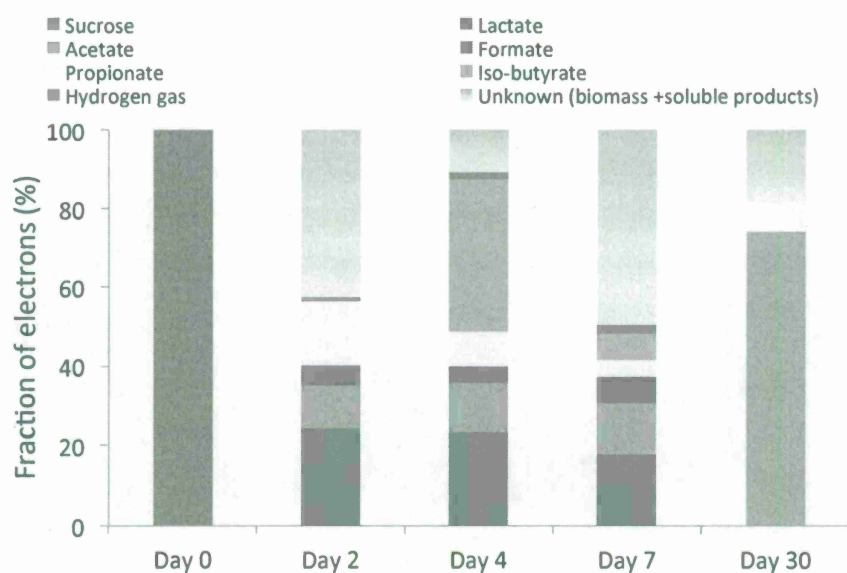


**Figure 6.1.** Electron flow distribution during batch (up to day 7) and subsequent semi-continuous (day 30) operation of fermentation reaction fed with sucrose. The electron balance shifted from lactate, acetate, formate, and propionate during batch operation to predominantly acetate during semi-continuous operation.



We obtained pellets from the suspension of the semi-continuous reactor after 2 months of steady-state operation. We extracted DNA from the pellets after freezing them overnight at -20 °C using RNeasy Blood and Tissue kit according to manufacturer's instructions along with modifications according to Ziv-El et al (2011). We quantified the extracted DNA using a Nanodrop spectrophotometer. We amplified the 16S rRNA gene for general bacteria using primers 8F and 1525R (Lane, 1991), after which the PCR products were purified for clone library preparation. We performed clone library analysis using TOPO TA cloning kit for sequencing, according to manufacturer's instructions. We sequenced the inserted PCR products and analyzed the closest match with BLAST software. A total of 63 clones were picked (Figure 6.2).

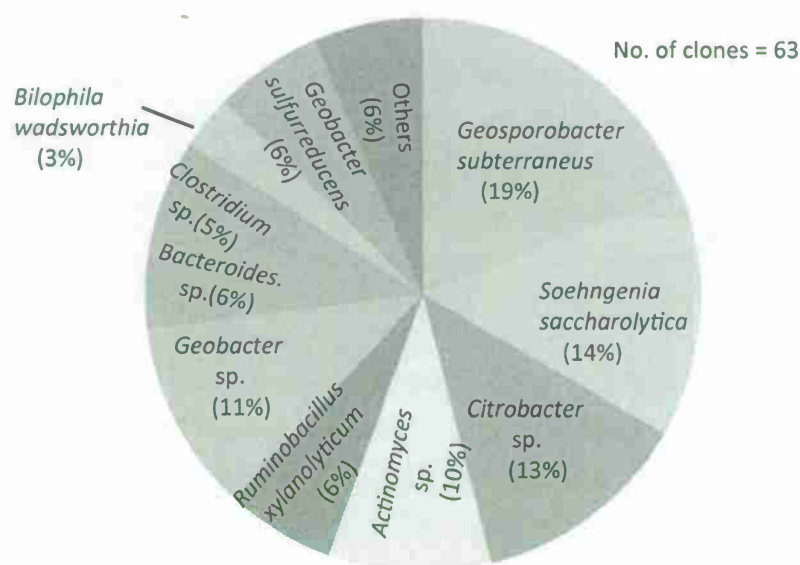


**Figure 6.2.** Clone library analysis based on the 16S rRNA for the sucrose enrichment culture that converted sucrose predominantly to acetate and some propionate.

The obligate anaerobic fermentative bacterium, *Geosporobacter subterraneus*, comprised around 19% of the total clones. *Geosporobacter* belongs to the *Clostridiales* order and it ferments sugars such as glucose and sucrose, to mainly acetate, H<sub>2</sub>, and CO<sub>2</sub> with a growth optimum temperature of 42 °C and pH of 7.3 (Klouche et al, 2007). *Soehngenia saccharolytica*, belonging to cluster XII of *Clostridia*, accounted for 14% of the clones - it is anaerobic, aerotolerant, and saccharolytic, with major end products of sugar fermentation being acetate, formate, H<sub>2</sub>, CO<sub>2</sub>, and ethanol (Parshina et al, 2003). *Citrobacter amalonaticus* (13% of total clones) belongs to the *Enterobacteriaceae* family and is known to perform biological water gas shift reaction to produce hydrogen gas from carbon monoxide (Robaire, 2006) when supplemented with glucose/sucrose as carbon source.

*Ruminobacillus xylanolyticum* is another known genus of heterotrophic homo-acetogens that possess the capability to produce acetate either from sugars or from  $H_2/CO_2$  (Drake HL, 1994). Since the enrichment was obtained from the suspension of an MEC anode, we also observed *Geobacter* sp. (11%) and *Geobacter sulfurreducens* (6%). However, their role towards sucrose fermentation is unclear. *Actinomyces* sp. (10% of total clones) and *Bacteroides* sp. (3%) are often associated with anaerobic biofilms such as MEC anodes. However, their role with respect to sucrose fermentation is also unknown.

To determine the possibility of achieving high Coulombic efficiencies from sucrose, the homo-acetogenic culture described above was combined with a highly enriched with *Geobacter* sp. in flat-plate MEC anodes producing high current densities (described in Section 4). We first acclimatized the acetate-fed ARB grown in the flat-plate MEC with 100 mM phosphate buffer solution to anaerobic media containing 100 mM  $NaHCO_3$ . After the medium change, a steady current density of  $300 A/m^3_{anode}$  was sustained for a few days under continuous mode of operation, at which point we shifted to batch mode so as to starve the biofilm (Figure 6.3). When the current density dropped to around 10% of the maximum value ( $\sim 30 A/m^3_{anode}$ ), we replaced the anode content with the basal sucrose enrichment medium through continuous flow, but without sucrose addition (Figure 6.3).

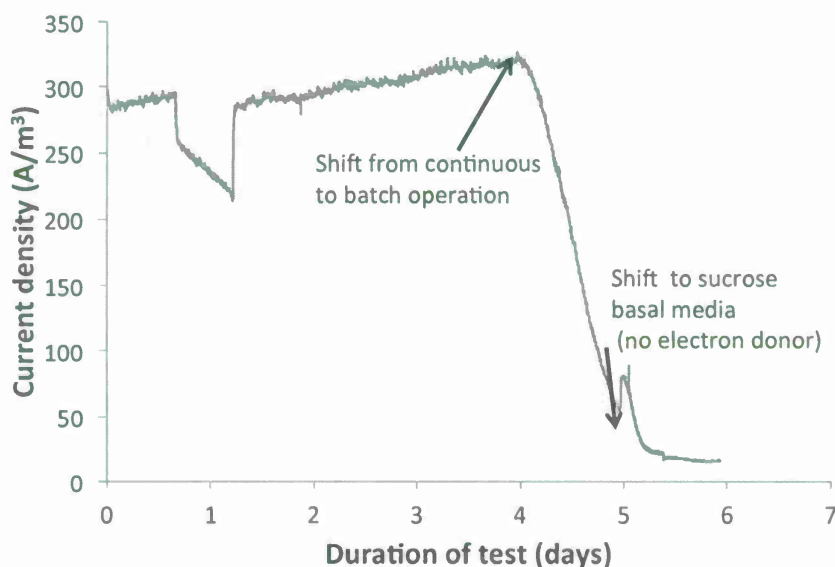


**Figure 6.3.** Volumetric current density for the acetate-fed flat plate MEC before the electron-balance experiment with the sucrose co-culture.

We started the electron balance experiment with the sucrose co-culture, after waiting for three HRTs (1 HRT = 9 hours) to ensure sufficient medium replacement. Then, we separately added a

pellet of the sucrose enrichment culture and 5 mM sucrose into the anode chamber. We obtained an initial sample from the MEC anode at time  $t = 0$  for quantifying the exact amount of sucrose and other organic acids by high performance liquid chromatography (HPLC) equipped with BIORAD Aminex HPX-87H column for sugars and volatile acids analysis. Sucrose analysis employed water as the eluent phase, while the column was kept at 30 °C and a refractive index detector (RID) served as the detector. We analyzed volatile acids and alcohols using methods described in Parameswaran et al (2009).

Current density increased instantaneously to 27 A/m<sup>3</sup> after the spike, and then it increased rapidly over the next several hours to reach a maximum value of 150 A/m<sup>3</sup> (Figure 6.4). This is half the maximum current density under acetate-fed conditions. The maximum current density was sustained for about 6 hours, after which it rapidly declined to stabilize around 20 A/m<sup>3</sup>. HPLC analysis indicated that the influent sucrose concentration was 5.6 ( $\pm 0.02$ ) mM, while no sucrose was detected at the end of the batch operation. We did not detect acetate or other volatile acids at the start or end of the batch run. Coulombic efficiency, based on sucrose removal, was 97% (Figure 6.4). Current from decaying biomass in the biofilm anode could be a significant fraction of the observed current density, as indicated by the tail end of Figure 6.4, which was still hovering around 20 A/m<sup>3</sup> for about 2 days. A conservative estimate of Coulombic efficiency after discarding all current density observed after 2.5 days still is 82%.

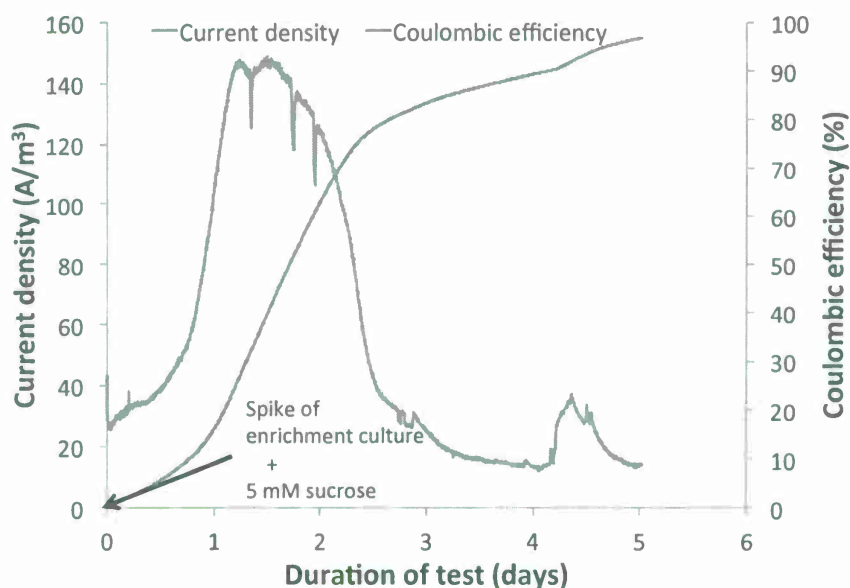


**Figure 6.4.** Batch sucrose co-culture MEC operation indicating the observed current density and Coulombic efficiency.



Recent research with sucrose- fed microbial fuel cells have shown Coulombic efficiencies ranging from 4% in single chamber MFCs (Beecroft et al., 2012) to a maximum of 92% in two-stage modular MFCs (Kim et al., 2010). Our results are a first documentation of very high Coulombic efficiency from sucrose during combined fermentation + anode respiration in a single-step MEC anode.

## 7. Summary and Conclusions

An MFC is a complex biological and electrochemical reactor in which different processes should be optimized in order to maximize current and power outputs. Throughout our project, we optimized materials, configurations, cathodic reactions, and microbial communities. The selection of anode materials proved to be an important parameter to optimize an MFC. Certain materials, such as stainless steel, reduce ARB performance and current production. On the other hand, the selection of an AEM that minimizes potential losses in an MFC yielded only a small improvement in the overall performance of the MFC. Our results show that most of the potential losses in an MFC occur at the cathode, where a pH gradient creates a concentration overpotential that can be responsible for the loss of up to ~30% of the energy available in an MFC. We provide a few strategies to minimize pH gradients and prevent potential losses.

Based on the analysis above, we built and tested a prototype MFC that produced up to 500 A/m<sub>anode</sub><sup>3</sup>. An important characteristic of our MFC prototype is the short distance between anode and cathode (< 0.5 cm). Based on our calculations, this short distance is required to achieve high power densities in an MFC. Longer distances between anode and cathode result in prohibitively large Ohmic losses that reduce the operating potential of the MFC.

Finally, we optimized a microbial community for the consumption of sucrose, achieving a Coulombic efficiency of > 90%. Our experiments show the importance of optimizing microbial communities in MFCs in order to maximize electron recoveries. Combining our individual results, we have made significant progress towards the development of an efficient sucrose-fed microbial fuel cell.

## References

- Beecroft NJ, Zhao F, Varcoe JR, Slade RCT, Thumser AE, Avignone-Rossa C. 2012. Dynamic changes in microbial community composition in microbial fuel cells fed with sucrose. *Appl Microbiol Biotechnol* 93: 423-437.
- Chaudhuri SK, Lovley DR. 2003. Electricity generation by direct oxidation of glucose in mediatorless microbial fuel cells. *Nat Biotechnol* 21(10): 1229-1232.
- Cheng S, Liu H, Logan BE. 2006. Increased performance of single-chamber microbial fuel cells using an improved cathode structure. *Electrochem Comm* 8:489-494.
- Drake HL. 1994. Acetogenesis. In Chapman and Hall Microbiology Series. London: Chapman Hall.
- Dumas C, Basseguy R, Bergel A. 2008. DSA to grow electrochemically active biofilms of *Geobacter sulfurreducens*. *Electrochim Acta* 53(7):3200-3209.
- Fan YZ, Hu HQ, Liu H. 2007. Sustainable power generation in microbial fuel cells using bicarbonate buffer and proton transfer mechanisms. *Environ Sci Technol* 42(23): 8154-8158.
- Fang J, Shen PK. 2006. Quaternized poly(phthalazinon ether sulfone ketone) membrane for anion exchange membrane fuel cells. *J Membrane Sci* 285(1-2): 317-322.
- Ha PT, Tae B, Chang IS. 2008. Performance and bacterial consortium of microbial fuel cell fed with formate. *Energy & Fuels* 22(1):164-168.
- He Z, Wagner N, Minteer SD, Angenent LT. 2006. An Upflow Microbial Fuel Cell with an Interior Cathode: Assessment of the Internal Resistance by Impedance Spectroscopy. *Environ Sci Technol* 40: 5212-5217.
- Inoue K, Leang C, Franks AE, Woodard TL, Nevin KP, Lovley DR. 2011. Specific localization of the c-type cytochrome OmcZ at the anode surface in current-producing biofilms of *Geobacter sulfurreducens*. *Environ Microbiol Reports* 3(2): 211-217.
- Kim JR, Oh SE, Cheng S, Logan BE. 2007. Power generation using different cation, anion and ultrafiltration membranes in microbial fuel cells. *Environ Sci Technol* 41(3): 1004-1009.
- Kim JR, Premier GC, Hawkes FR, Rodriguez J, Dinsdale RM, Guwy AJ. 2010. Modular tubular microbial fuel cells for energy recovery during sucrose wastewater treatment at low organic loading rate. 101: 1190-1198.
- Klouche N, Fardea ML, Lascourrèga JF, Cayo JL, Hacen H, Thomas P, Magot M. 2007. *Geosporobacter subterraneus* sp. nov., a spore forming bacterium isolated from a deep subsurface aquifer. *Int J Syst Evol Microbiol* 57: 1757-1761.
- Lane DJ. 1991. 16S/23S rRNA sequencing. In: Stackebrandt, E., Goodfellow, M. (Eds), *Modern microbiological methods*. Wiley, Chichester, New York, pp: 115-175.
- Lee HS, Rittmann BE. 2010. Significance of Biological Hydrogen Oxidation in a Continuous Single-Chamber Microbial Electrolysis Cell. *Environ Sci Technol* 44: 948-954.
- Liu H, Cheng SA, Logan BE. 2005. Production of electricity from acetate or butyrate using a single-chamber microbial fuel cell. *Environ Sci Technol* 39(2): 658-662.

- Logan BE, Hamelers B, Rozendal RA, Schröder U, Keller J, Freguia S, Aelterman P, Verstraete W, Rabaey K. 2006. Microbial fuel cells: Methodology and technology. *Environ Sci Technol* 40:5181–5192.
- Logan BE, Cheng S, Watson V, Estadt G. 2007. Graphite Fiber Brush Anodes for Increased Power Production in Air-Cathode Microbial Fuel Cells. *Environ Sci Technol* 41(9):3341-3346.
- Marcus AK, Torres CI, Rittmann BE. 2007. Conduction-based modeling of the biofilm anode of a microbial fuel cell. *Biotechnol Bioeng* 98(6):1171-1182.
- Parameswaran P, Torres CI, Lee HS, Krajmalnik-Brown R, Rittmann BE. 2009. Syntrophic interactions between anode-respiring bacteria (ARB) and non-ARB in a biofilm anode: electron balances. *Biotech Bioeng* 103(3): 513-523.
- Parameswaran P, Torres CI, Lee HS, Rittmann BE, Krajmalnik-Brown R. 2011. Hydrogen consumption in microbial electrochemical systems (MXCs): The role of homo-acetogenic bacteria. *Bioresource Technol* 102(1): 263-271.
- Parshina SN, Kleerebezem R, Sanz JL, Letting G, Nozhevnikova AN, Kostrikina NA, Lysenko AM, Stams AJM. 2003. *Soehngenia saccharolytica* sp. nov. and *Clostridium amygdalinum* sp. nov., two novel anaerobic benzaldehyde-converting bacteria. *Int J Syst Evol Microbiol* 53: 1791-1799.
- Perlack RD, Wright LL, et al. 2005. Biomass as Feedstock for a bioenergy and bioproducts industry: the technical feasibility of a billion-ton annual supply. U.S. DOE/USDA report.
- Piela P, Wrona PK. 2006. Some anion-transport properties of Nafion (TM) 117 from fuel cell hydrogen peroxide generation data. *J Power Sources* 158(2): 1262-1269.
- Richter H, McCarthy K, Nevin KP, Johnson JP, Rotello VM, Lovley DR. 2008. Electricity generation by *Geobacter sulfurreducens* attached to gold electrodes. *Langmuir* 24: 4376- 4379.
- Rismani-Yazdi H, Carver SM, Christy AD, Tuovinen IH. 2008. Cathodic limitations in microbial fuel cells: An overview. *J Power Sources* 180(2): 683-694.
- Robaire, S. Master's thesis, 2006. Biological hydrogen production using *Citrobacter amalonaticus* Y19 to catalyze the water gas shift reaction. The University of British Columbia
- Rozendal RA, Hamelers HVM, Molenkmp RJ, Buisman CJN. 2007. Performance of single chamber biocatalyzed electrolysis with different types of ion exchange membranes. *Water Res* 41: 1984-1994.
- Rozendal RA, Hamelers HVM, Rabaey K, Keller J, Buisman CJN. 2008. Towards practical implementation of bioelectrochemical wastewater treatment. *Trends Biotechnol* 26(8): 450-459.
- Sleutels THJA, Hamelers HVM, Rozendal RA, Buisman CJN. 2009. Ion transport resistance in Microbial Electrolysis Cells with anion and cation exchange membranes. *Int J Hydrogen Energy* 34(9): 3612-3620.
- Ter Heijne A, Hamelers HVM, De Wilde V, Rozendal RA, Buisman CJN. 2006. A bipolar membrane combined with ferric iron reduction as an efficient cathode system in microbial fuel cells. *Environ Sci Technol* 40:5200-5205.
- Torres CI, Marcus AK, Rittmann BE. 2007. Kinetics of Consumption of Fermentation Products by Anode-Respiring Bacteria. *Appl Microbiol Biot* 77(3): 689-697.



- Torres CI, Marcus AK, Parameswaran P, Rittmann BE. 2008a. Kinetic experiments for evaluating the Nernst-Monod model for anode-respiring bacteria (ARB) in a biofilm anode. *Environ Sci Technol* 42(17): 6593-6597.
- Torres CI, Marcus AK, Rittmann BE. 2008b. Proton transport inside the biofilm limits electrical current generation by anode-respiring bacteria. *Biotechnol Bioeng*. 100(5): 872-881.
- Torres CI, Lee HS, Rittmann BE. 2008c. Carbonate species as OH<sup>-</sup> carriers for decreasing the pH gradient between cathode and anode in biofuel-cells. *Environ Sci Technol* 42(23): 8773- 8777.
- Torres CI, Krajmalnik-Brown R, Parameswaran P, Marcus AK, Wanger G, Gorby YA, Rittmann BE. 2009. Selecting anode-respiring bacteria based on anode potential: Phylogenetic, electrochemical and microscopic characterization. *Environ Sci Technol* 43(24): 9519-9524.
- U.S. Department of Energy, Office of the Biomass Program. 2009. Multiyear Program Plan 2007-2017.
- Varcoe JR, Slade RCT. 2005. Prospects for alkaline anion-exchange membranes in low temperature fuel cells. *Fuel Cells* 5(2): 187-200.
- Varcoe JR, Slade RCT, Lam How Yee E. 2006. An alkaline polymer electrochemical interface: a breakthrough in application of alkaline anion-exchange membranes in fuel cells. *Chem Comm* 13:1428-1429.
- Warner J, Singer PW. 2009. *Fueling the Balance: A Defense Energy Strategy Primer*, Foreign Policy at Brookings.
- Xiong Y, Fang J, Zeng QH, Liu QL. 2008. Preparation and characterization of cross-linked quaternized poly(vinyl alcohol) membranes for anion exchange membrane fuel cells. *J Membrane Sci* 311(1-2): 319-325.
- Zhang F, Merrill MD, Tokash JC, Saito T, Cheng S, Hickner MA, Logan BE. 2011. Mesh optimization for microbial fuel cell cathodes constructed around stainless steel mesh current collectors. *J Power Sources*. 196(3):1097–1102.
- Zhang X, Cheng S, Huang X, Logan BE. 2010. Improved performance of single-chamber microbial fuel cells through control of membrane deformation. *Biosen Bioelectron* 25(7):1553-1858.
- Zhao F, Harnisch F, Schroeder U, Scholz F, Bogdanoff P, Herrmann I. 2006. Challenges and constraints of using oxygen cathodes in microbial fuel cells. *Environ Sci Technol* 40(17): 5193-5199.
- Ziv-El M, Delgado AG, Yao Y, Kang DW, Nelson KG, Halden RU, Krajmalnik-Brown R. 2011. Development and characterization of DehaloR<sup>2</sup>, a novel anaerobic microbial consortium performing rapid dechlorination to ethene. *Appl Microbiol Biotechnol* 92: 1063-1071.